Electronic Supplementary Material (ESI) for Catalysis Science & Technology.

Electronic Supplementary Information

Prediction of optimal catalysts for a given chemical reaction

Hervé Toulhoat[1]*, Pascal Raybaud[2]

[1] Sorbonne Université, UPMC, CNRS, Laboratoire de Réactivité de Surface, 4 Place Jussieu, 75005, Paris, France.

[2] IFP Energies nouvelles, Rond-point de l'Echangeur de Solaize, BP 3, 69360, Solaize, France.

*Correspondence to: herve.toulhoat@orange.fr

Table of contents

1- Correlation between E_{MO} and occupancy of antibonding orbitals of e_g parentage in the coordination sphere of transition metal cations in oxides

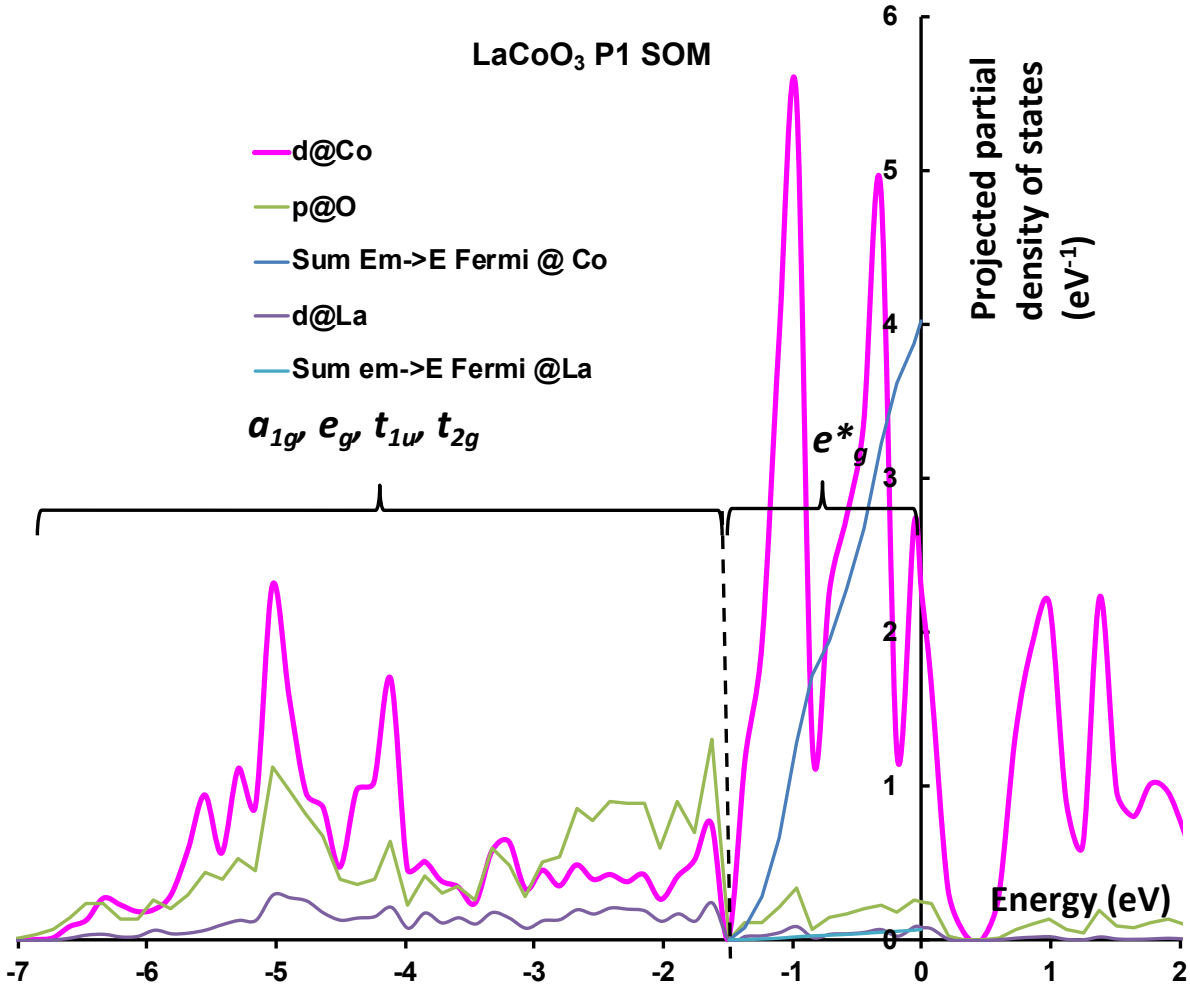

Fig. S.1.1: Example of projected partial density of states (sum of spin up and spin down contributions) which form the basis for the calculation the number of d electrons $N_{e*g}{}^{@M}$ occupying orbitals of e^*_g parentage: it corresponds to the intersection of the blue integral curve with the Y axis (at Fermi level, Energy = 0).

Table ST.1.1: Results of E_{MO} and $N_{e*_g@M}$ calculations for the set of oxides considered in Figures. 2 and 3 of main text

Formula	***Space group***	***Target atom M***	Z	E_{MX} ***(kJ.Mol^{-1})***	$N_{e*_g@M}$
La_2NiO_4	Bmab	Ni	6	117.5	5.18
La_2MnNiO_6	$P2_1/m$	Ni	6	132.4	4.92
$La_4Ni_3O_{10}$	Fmmm	Ni	6	137.9	4.60
$LaNiO_3$	R-3ch	Ni	6	147.3	4.24
$LaCoO_3$	R-3ch	Co	6	160.4	4.02
$LaFeO_3$	Pnma	Fe	6	165.9	3.58
$BaCoO_3$	Pm-3m	Co	6	172.6	3.31
$SrCoO_3$	Pm-3m	Co	6	172.8	3.10
$LaMnO_3$	Pnma	Mn	6	175.8	2.89
La_2MnNiO_6	$P2_1/m$	Mn	6	182.7	2.41
$LaCrO_3$	Pm-3m	Cr	6	183.1	2.72
$CaLaFe_2O_6$	$Pnm2_1$	Fe	6	183.7	2.80

2- *Volcano patterns for OER and ORR reactions against E_{MO} in transition metal oxides.*

Table ST.2.1 and ST.2.2 gather E_{MO} at the SOC level, and specific catalytic activity data for oxyde catalysts of OER or POER reactions, and ORR reactions respectively. Figures 1 of the main text and figures S2.1 and S2.2 were built on the basis of these data.

The "volcanoes" in Figures 1a) and 1b) of main text are approximated by the intersecting regression lines corresponding to the left side and right side subsets of data points which can be rather clearly separated in all cases, and are defined in Tables ST.2.1 and ST.2.2. Abscissae of the intersection points of these lines provide the optimal value of the descriptor $E_{MO,opt}$ in all cases. The uncertainty $\Delta E_{MO,opt}$ on this value can be estimated by the interval between abscissae of intersection points of upper left with lower right on the one hand, and lower left with upper right on the other hand, bracketing lines (dotted on figures). Bracketing lines of a given regression line have the same slopes but standard deviation of experimental ordinates with respect to their projection on the corresponding regression line are added or subtracted to intercepts. The uncertainty ΔActivity max on the optimal activity can accordingly be estimated by the interval between ordinates of upper left and lower left bracketing lines at abscissa $E_{MO,opt}$. Table ST.2.3 gather the slopes, intercepts and squared coefficients for these regression lines, as well as the coordinate of optimal intersections and the above defined uncertainties.

We conclude most importantly that the abscissae of volcanoes summit differ only by at most 5 kJ.Mol^{-1}, which is lower than the expected accuracy on E_{MO} which combines the output of three separated DFT calculations, when results of different groups are considered (OER, POER and ORR A and B), or when outlying data points are reinterpreted. We adopt therefore $E_{MO,opt} = 179 \pm 2$ kJ.Mol^{-1} for OER and POER, and 170 ± 4 kJ.Mol^{-1} for ORR.

Table ST.2.1: Comparison of experimental activities and calculated E_{MO} values with spin orbit coupling for oxides catalysts of OER and POER considered in Fig. 1 of main text (a): BSCF is approximated by $Sr_{62}Ba_{63}Fe_{25}Co_{100}O_{375}$ built by random substitutions in a supercell of $CaTiO_3$ (space group Pm-3m)) ; (b) average coordination number *Z* for target atom; (c) from ref [16] and [17] of main text, Fig S1 of Supporting online materials, in Volts versus RHE at 50 μA.cm^{-2}; (d) from ref [18] and [19] of main text, in $\log_{10}$ of $\mu molO_2.dm^{-3}.mn^{-1}$

Formula	***Space group***	***Target atom M***	*Z*	E_{MO} ***(kJ.Mol^{-1})***	**Activity**
OER left side					(c)
$LaNiO_3$	R-3ch	Ni	6	147.3	1.55
$LaCoO_3$	R3-ch	Co	6	160.4	1.58
$BaCoO_3$	Pm-3m	Co	6	172.8	1.48
BSCF(a)	P1	Co	6	172.6	1.48
$SrCoO_3$	Pm-3m	Co	6	172.8	1.48
OER right side					(c)
$CaLaFe_2O_6$	$Pnm2_1$	Fe	6	183.7	1.54
IrO_2	P42/Mnm	Ir	3	181.9	1.56
La_2MnNiO_6	$P2_1/m$	Mn	6	182.7	1.57
RuO_2	P42/Mnm	Ru	3	186.0	1.60
$LaCrO_3$	Pbnm	Cr	6	188.8	1.76
POER left side					(d)
NiO	Fm-3m	Ni	6	75.6	0.079
MgO	Fm-3m	Mg	6	132	0.5058
Rh_2O_3	R-3c	Rh	6	122.4	1.193
Co_2NiO_4	Fd-3m	Co	4	139.7	1.149
Mn_2O_3	Pbca	Mn	6	151.2	1.185
Co_3O4	Fd-3m	O	5.33(b)	134.3	1.407
POER right side					(d)
IrO_2	$P4_2/mnm$	Ir	3	181.9	1.436

RuO_2	$P4_2/mnm$	Ru	3	186.0	1.274

Table ST.2.2: Comparison of experimental activities and E_{MO} values calculated with spin orbit coupling for oxides catalysts of ORR considered in main text: (a) ORR A after ref [17] of main text, in Volts versus RHE at 50 μA.cm^{-2} and (b) ORR B after ref [21] of main text, in cm^2.mA^{-1} extrapolated at ω=0 ; (c) significant component retained for the sample described as a mixture of $LaNiO_3$ and $La_4Ni_3O_{10}$; (d) averaged between E_{NiO} and E_{CrO}.

Formula	***Space group***	***Target atom M***	Z	E_{MO} ***(kJ.Mol^{-1})***	**Activity**
ORR A left side					(a)
La_2NiO_4	Fm-3m	Ni	6	117.5	0.72
$La_4Ni_3O_{10}$	Fmmm	Ni	6	137.9	0.77
PtO_2	Pm-3m	Pt	6	146.6	0.96
$LaNiO_3$	R-3ch	Ni	6	147.3	0.91
$LaCoO_3$	R-3c	Co	6	160.4	0.85
ORR A right side					(a)
$LaMnO_3$	Pnma	Mn	6	175.8	0.84
La_2MnNiO_6	$P2_1/m$	Mn	6	182.7	0.77
$CaLaFe_2O_6$	$Pnm2_1$	Fe	6	183.7	0.70
$LaCrO_3$	Pbnm	Cr	6	188.8	0.68
ORR B left side					(b)
La_2FeNiO_6	$P2_1/m$	Ni	6	125.6	0.53
La_2CoNiO_6	$P2_1/m$	Ni	6	135.5	0.39
$La_4Ni_3O_{10}$ (c)	Fmmm	Ni	6	137.9	0.42
PtO_2	Pm-3m	Pt	6	146.6-	0.055
La_2CrNiO_6	$P2_1/m$	Cr,Ni(d)	6	154.6	0.35
$LaCoO_3$	R-3c	Co	6	160.4	0.15
ORR B right side					(b)
$LaMnO_3$	Pnma	Mn	6	175.8	0.24
La_2MnNiO_6	$P2_1/m$	Mn	6	182.7	0.28
$LaCrO_3$	Pm-3m	Cr	6	188.8	0.69

Table ST.2.3: Parameters of regression lines defining the 2 volcano plots for OER and POER shown on Fig. 1 of main text and the two volcano plots for ORR shown on Fig. S.2.1 and S.2.2. Intercepts b and Activity max in units of Activity mentioned for the corresponding sections of Tables ST.2.1 and ST.2.3; R^2: squared correlation coefficients; $E_{MO,opt}$and $\Delta E_{MO,opt}$in $kJ.mol^{-1}$; slopes m in units of Activity.kJ^{-1}.mol.

	OER left side	***OER right side***		***POER left side***	*POER right side*
m	0.0283	-0.003321		0.015	-0.039
b	-3.625	2.061		-0.990	8.58
R^2	0.8079	0.66853		0.6117	1 (2 data)
$E_{MO,opt}$	179.6			175.7	
$\Delta E_{MO,opt}$	1.5 (0.8%)			5.2 (2.9%)	
Activity max	1.465			1.67	
ΔActivity max	0.02			0.28	
	ORR A left side	***ORR A right side***		***ORR B left side***	***ORR B right side***
m	0.0043	-0.0128		-0.0098	0.0337
b	0.230	3.082		1.714	-5.744
R^2	0.4842	0.8850		0.5117	0.767
$E_{MO,opt}$	166.9			171.7	
$\Delta E_{MO,opt}$	4.2(2.5%)			4.09(2.4%)	
Activity max	0.95			0.038	
ΔActivity max	0.06			0.09	

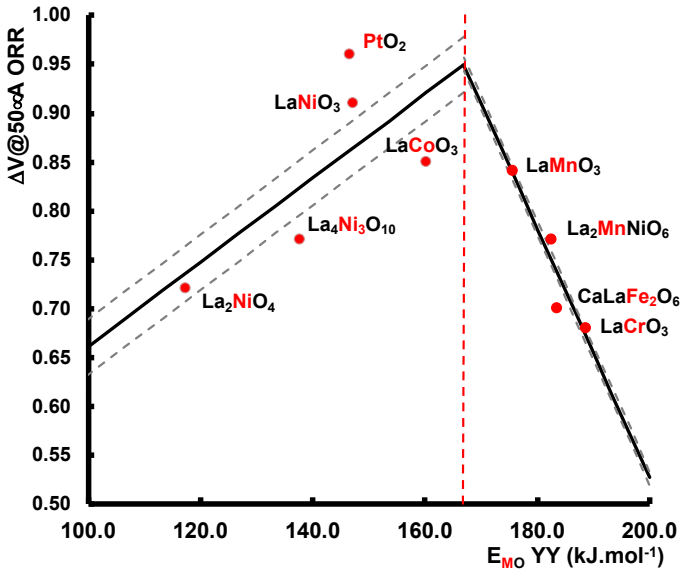

Fig. S.2.1: Volcano plot for ORR A.

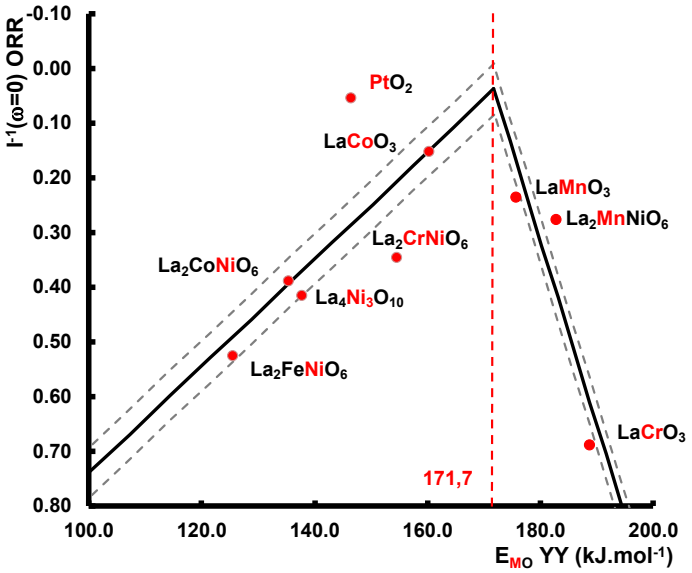

Fig. S.2.2: Volcano plot for ORR B.

3- *Volcano pattern for the hydrogen evolution reaction (HER) at transition metal cathodes against E_{MH} in transition metal hydrides.*

The most complete review of activities of transition metals as electro-catalysts for the hydrogen evolution reaction (HER) can be found in the work of S. Trasatti (ref. [22] of main text). Some data on single crystals were later included in the comparisons, as in the recent compilation by Greeley et al. [23]. In these compilations, specific electro-catalytic activities of metals cathodes for HER are normalized as $i_{0,H}$ meaning current per unit area of cathode (current densities in A.cm^{-2}), at equilibrium potential, i.e. 0V versus the Standard Hydrogen Electrode (SHE).

We have estimated the stable structures of metal hydrides in these testing conditions from predominance diagrams when data were available [34] or from the minimal computed heats of formation in order to discriminate between identical stoichiometries. For these structures, E_{MH} values have been computed including spin orbit coupling.

Table ST.3.1 presents the relevant results and Figure S.3.1 the resulting volcano plot for the HER in terms of $\ln(i_{0,H})$ versus E_{MH}. Table ST.3.2 provides the parameters for the regression lines defining this plot and its optimum.

Table ST.3.1: Comparison of experimental activities in HER and calculated E_{MH} values for transition elements electrocatalysts. (a) Activities from ref. [22] and [23] of main text below expressed as $\ln(i_{0,H})$, with $i_{0,H}$ in A.cm^{-2}

Formula	*Space group*	*Target atom*	*Z*	E_{MH} *(kJ.Mol^{-1})*	**Activity**
Left side					(a)
AuH	Fm-3m	H	6	25.0	-6.5
AgH	Fm-3m	H	6	26.6	-5.0
OsH	Fm-3m	H	6	28.8	-4.1
IrH	Fm-3m	H	6	30.4	-3.6
Pt_2H	I4_1/amd	H	6	31.1	-3.0
Right side					(a)
ReH	Fm-3m	H	6	34.3	-3.0
Rh_2H	I4_1/amd	H	6	37.3	-3.5
FeH	Fm-3m	H	6	39.1	-5.6
RuH	Fm-3m	H	6	40.3	-4.2
Pd_2H	I4_1/amd	H	6	40.8	-3.7
NiH	Fm-3m	H	6	41.5	-5.3
CoH	Fm-3m	H	6	41.8	-5.3
WH	P6_3/mmc	H	6	43.7	-6.4
TaH	Pnnn	H	6	46.5	-8.5
NbH	Pnnn	H	6	47.5	-8.4
MoH	P6_3/mmc	H	6	48.3	-7.3
TiH	Fm-3m	H	6	50.4	-8.3
CrH	P6_3/mmc	H	6	50.6	-7.4
MnH_2	Fm-3m	H	4	54.3	-10.9
CuH	Fm-3m	H	6	34.0	
CuH	P6_3mc	H	4	59.4	
Average				*46.7*	-7.8

Table ST.3.2: Parameters of regression lines defining the volcano plot shown on Fig. S.3.1, for HER. Intercepts b and Activity max in $\ln(i_{0,H})$, with $i_{0,H}$ in A.cm^{-}; R^2 : squared correlation coefficients; $E_{MH,opt}$ in *kJ.mol^{-1};* slopes m in units of $\ln(i_{0,H})$.kJ^{-1}.mol.

	HER left side	*HER right side*
m	0.525	-0.375
b	-19.337	10.254
R^2	0.9584	0.8667
$E_{MH,opt}$	32.9	
$\Delta E_{MH,opt}$	0.3 (0.9 %)	
Activity max	-2.08	

ΔActivity max	0.3	

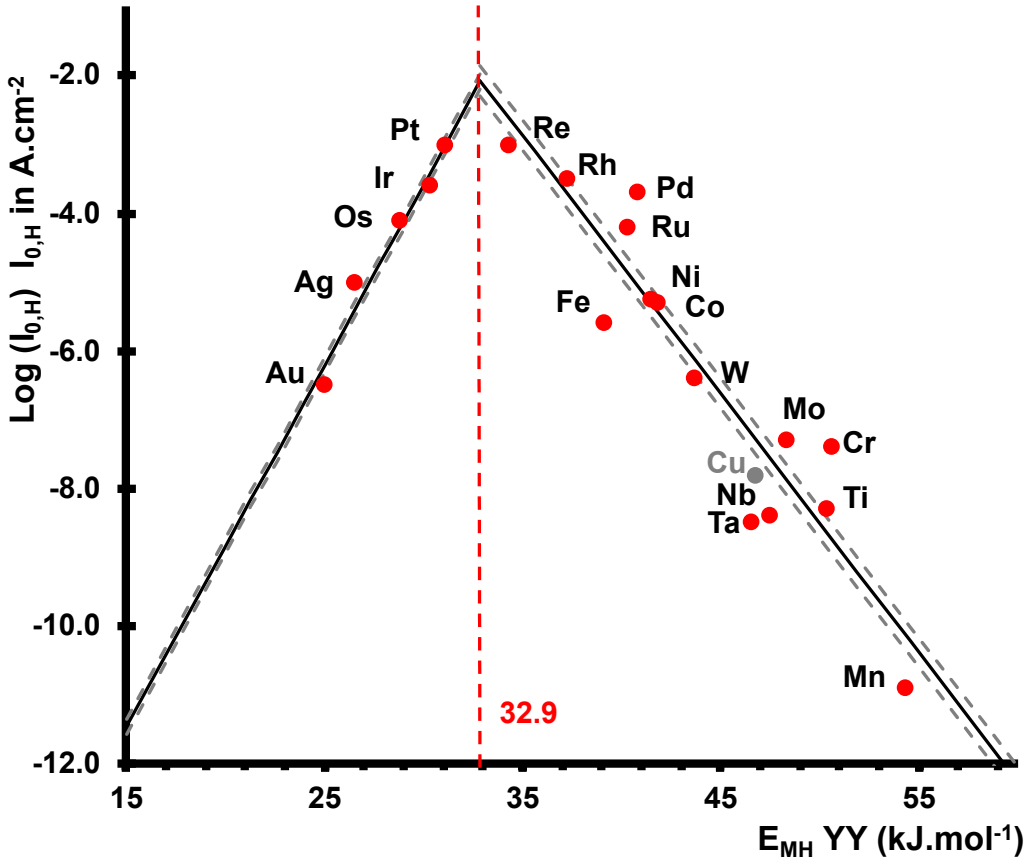

Fig. S.3.1: Volcano plot for HER on transition metals. Dotted lines bracket the regression lines by ± the standard deviation of experimental ordinates with respect to their projection on the left or right regression line, allowing estimations of error bars on the coordinates of the volcano summit as situated between cross-points of left+/right- and left-/right+. The data point for Cu is not included in the right hand side regression, since its abscissa is tentatively taken as the average of E_{MH} for CuH Fm-3m (Z_{Cu}=6) and CuH P6_3mc (Z_{Cu}=4).

4- Volcano patterns for hydrodesulfurization of thiophene and hydrogenation of biphenyl against E_{MS} in transition metal sulfides.

Our volcano patterns for thiophene hydrodesulfurization and hydrogenation of biphenyl are reconsider published experimental activity data for unsupported transition metal sulfide catalysts (TMS) by Lacroix et al. in references [25], [26] and [27] from main text, and are similar to figures 1.7 and 1.9 of reference [24] from main text. In the latter reference are described the procedures to determine the stable TMS structures in testing conditions for which E_{MS} Yin-Yang descriptors were computed, and to normalize activities into turnover frequencies. We now report slight differences with our previous analysis, after a more careful inspection of thermodynamic stability diagrams for TMS in test conditions, including spin orbit magnetic coupling in the DFT calculations of E_{MS}. For thiophene hydrodesulfurization Table ST.4.1 presents the relevant data, and Figure 4 a) of main text the resulting volcano plot. Table ST.4.2 provides the parameters for the regression lines defining this plot and its optimum. For hydrogenation of biphenyl, Table ST.4.3 presents the relevant data, and Figure S.4.1 the resulting volcano plot. Table ST.4.4 provides the parameters for the regression lines defining this plot and its optimum. We obtain $E_{MS,opt}$ = 137.3 ± 3 kJ.Mol^{-1} for thiophene hydrodesulfurization and $E_{MS,opt}$ = 122.2 ± 4 kJ.Mol^{-1} for hydrogenation of biphenyl. These values remain within error margins identical to those reported in figures 1.7 and 1.9 of [24], i.e. 133.8 ± 3 and 121.2 ± 3 kJ.Mol^{-1} respectively

Table ST.4.1: Comparison of experimental activities and calculated E_{MS} values (Spin Orbit Coupling level) for unsupported transition elements sulfide catalysts of thiophene hydrodesulfurization considered in Fig. S.4.1 (a) Activities from ref. [25], [26] and [27] in main text, being expressed as turnover frequencies in s^{-1}. For Co_9S_8, only 6-fold coordinated Co atoms are assumed active (1/9).

Formula	*Space group*	*Target atom M*	*Z*	E_{MS} *(kJ.Mol^{-1})*	**Activity**
Left side					(a)
Pd_4S	P-42$_1$c	Pd	6	61.4	1.29E-04
NiS	P6_3/mmc	Ni	6	76.0	4.78E-05
MnS	Fm-3m	Mn	6	84.9	8.05E-05
CrS	P-31c	Cr	6	89.4	4.70E-04
VS	P6_3/mmc	V	6	95.4	1.57E-03
Fe_7S_8	C2	Fe	6	101.4	2.58E-03
Co_9S_8	Fm-3m	Co	6	112.6	5.07E-03
Rh_3S_4	C2/m	Rh	6	119.3	8.34E-03
Right side					(a)
RuS_2	Pa-3	Ru	6	138.7	4.34E-02
MoS_2	P6_3/mmc	Mo	6	167.9	6.01E-03
TiS_2	P-3m1	Ti	6	176.0	5.35E-04
NbS_2	R3m	Nb	6	177.3	2.36E-03
ZrS_2	P-3m1	Nb	6	199.9	3.72E-04

Table ST.4.2: Parameters of regression lines defining the volcano plot shown on Fig. 4a) of main text, for thiophene hydrodesulfurization. Intercepts b in $\log_{10}$(Activity units of s^{-1}) and Activity max in s^{-1}; R^2: squared correlation coefficients; $E_{MS,opt}$ in *kJ.mol^{-1};* slopes m in units of $\log_{10}$(Activity).kJ^{-1}.mol.

.

	thiophene hydrodesulfurization left side	*thiophene hydrodesulfurization right side*
m	0.0406	-0.0353
b	-6.93	3.488
R^2	0.8026	0.8617
$E_{MS,opt}$	137.3	
$\Delta E_{MS,opt}$	3.3 (2.5%)	
Activity max	4.37E-02	
ΔActivity max	7E-03	

Table ST.4.3: Comparison of experimental activities and calculated E_{MS} values (Spin Orbit Coupling level) for unsupported transition elements sulfide catalysts of hydrogenation of biphenyl considered in Fig. S.4.2 (a) Activities from ref [27] in main text, being expressed as turnover frequencies in s^{-1}. For Co_9S_8, only 6-fold coordinated Co atoms are assumed active (1/9).

Formula	*Space group*	*Target atom M*	*Z*	E_{MS} *(kJ.Mol^{-1})*	**Activity**
Left side					(a)
Pd_4S	P-42_1c	Pd	6	61.4	3.87E-05
FeS	P2_1/m	Fe	6	67.7	3.48E-05
NiS	P6_3/mmc	Ni	6	76.0	5.19E-05
MnS	Fm-3m	Mn	6	84.9	1.61E-05
CrS	P6_3/mmc	Cr	6	89.4	1.47E-04
VS	P6_3/mmc	V	6	95.4	4.87E-04
Co_9S_8	Fm-3m	Co	6	112.6	1.99E-04
$Rh_{17}S_{15}$	C2/m	Rh	6	114.1	1.31E-03
NbS_3	P-1	Nb	6	132.5	2.08E-03
Right side					(a)
RuS_2	Pa-3	Ru	6	138.7	1.45E-03
ReS_2	P6_3/mmc	Re	6	156.5	5.70E-04
MoS_2	P6_3/mmc	Mo	6	167.9	4.71E-04
WS_2	P6_3/mmc	W	6	173.0	3.28E-04
TiS_2	P-3m1	Ti	6	176.0	6.75E-05
ZrS_2	P-3m1	Zr	6	199.9	3.47E-05

Table ST.4.4: Parameters of regression lines defining the volcano plot shown on Fig. S.4.2, for hydrogenation of biphenyl. Intercepts b in $\log_{10}$(Activity units of s^{-1}) and Activity max in s^{-1}; R^2: squared correlation coefficients; $E_{MS,opt}$ in $kJ.mol^{-1}$; slopes m in units of $\log_{10}$(Activity).kJ^{-1}.mol.

	hydrogenation of biphenyl left side	*hydrogenation of biphenyl right side*
m	0.0325	-0.017
b	-6.602	-0.563
R^2	0.9459	0.52794
$E_{MS,opt}$	122.2	
$\Delta E_{MS,opt}$	3.8 (3%)	
Activity max	2.34E-03	
ΔActivity max	6E-04	

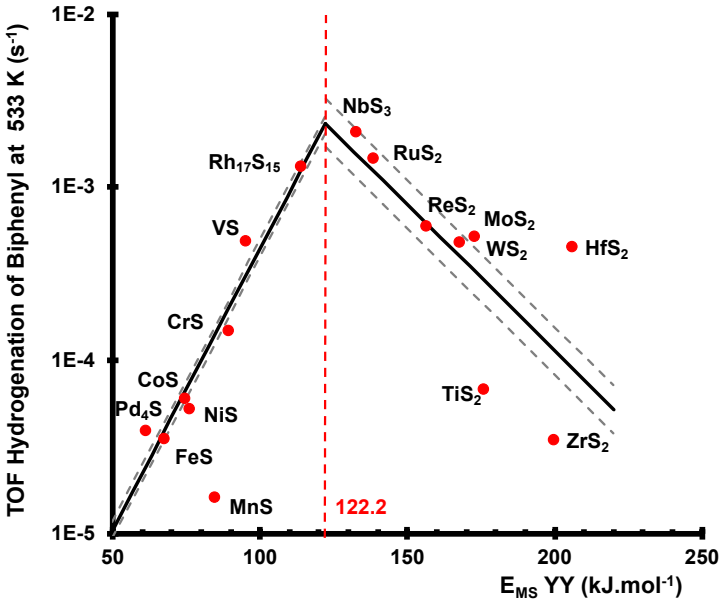

Fig. S.4.1: Volcano plot for hydrogenation of biphenyl over unsupported transition elements sulfides

5- *Volcano pattern for ammonia synthesis and decomposition against E_{MN} in transition metal nitrides*

To build a volcano pattern for ammonia synthesis we rely on experimental activity data provided by Ozaki et al. (ref [28] of main text) for K promoted carbon supported transition elements under the stoichiometric reactant mixture $3H_2+N_2$ at atmospheric pressure at 573 K.

E_{MN} descriptors were computed at the Spin-Orbit Coupling level, for the stable structures of metal nitrides in the test conditions, according to predominance diagrams when data were available [34] or according to the minimal computed heats of formation in order to discriminate between identical stoichiometries.

Table ST.5.1 presents the relevant results and Fig. 4b) of main text the illustrates the resulting volcano plot. Table ST.5.2 provides the parameters for the regression lines defining this plot and its optimum. Uncertainties were estimated as described in section 2 above. We determine therefore for NH_3 synthesis $E_{MN,opt} = 95 \pm 5$ kJ.mol^{-1}.

Table ST.5.1: Comparison of experimental activities and calculated E_{MN} values for K promoted carbon supported transition elements catalysts of NH_3 synthesis considered in Fig. 2 b) of main text (a) Activities adapted from ref [28] of main text, being expressed in units of 10^{-5}.mol NH_3.mol^{-1}metal.s^{-1}, assuming similar dispersions of active phase for all catalysts.

Formula	*Space group*	*Target atom M*	*Z*	E_{MN} *(kJ.Mol^{-1})*	**Activity**
Left side					(a)
PtN_2	Pnnm	Pt	6	65.8	3.87E-02
NiN_2	Pnnm	Ni	6	48.7	5.82E-02
CoN_2	Pnnm	Co	6	63.9	5.846E-01
IrN_2	Pnnm	Ir	6	79.6	3.24E+00
Rh_2N	P6_3/mmc	Rh	6	77.9	1.327E+00
Ru_2N	P6_3/mmc	Ru	6	93.4	5.62E+01
OsN_2	Pnnm	Os	6	96.3	2.64E+01
Right side					(a)
Ru_2N	P6_3/mmc	Ru	6	93.4	5.62E+01
OsN_2	Pnnm	Os	6	96.3	2.64E+01
Re_2N	P6_3/mmc	Re	6	107.2	1.66E+00
Fe_2N	Pbcn	Fe	6	114.2	9.973E-01
MoN	P63mc	Mo	6	120.0	1.428E+00

Table ST.5.2: Parameters of regression lines defining the volcano plot shown in Figure 2b), for NH_3 synthesis, Intercepts b and Activity max in Activity units of 10^{-5}.mol NH_3.mol^{-1}Metal.s^{-1} at 573K, under 600 Torr, $3H_2+N_2$ mixture; R^2: squared correlation coefficients; $E_{MN,opt}$ in kJ.mol^{-1}; slopes m in units of activity.kJ^{-1}.mol.

	NH_3 synthesis left side	*NH_3 synthesis right side*
m	0.0658	-0.0659
b	-4.805	7.712
R^2	0.8448	0.8560
$E_{MN,opt}$	95.03	
$\Delta E_{MN,opt}$	4.4 (4.6%)	
Activity max	1.446	
ΔActivity max	0.25	

To build a volcano pattern for ammonia decomposition, we rely on experimental activity data recently provided by Ganley et al. (ref [30] of main text) for activated alumina supported transition elements under pure NH_3 at atmospheric pressure and 853 K. In these

careful experiments, ammonia decomposition rates were measured in differential conversion conditions, and normalized in terms of turnover frequencies (TOF, s^{-1}) according to measured dispersions of the supported transition elements.

We have estimated the stable structures of metal nitrides in these test conditions from predominance diagrams when data were available [34] or from the minimal computed heats of formation in order to discriminate between identical stoichiometries. There are some differences compared to test conditions of ammonia synthesis. E_{MN} descriptors of NH_3 decomposition were computed for these stable structures.

Table ST.5.3 presents the relevant results and Figure S.5.1 the resulting volcano plot, to be compared with that for NH_3 synthesis on figure 2b). Table ST.5.4 provides the parameters for the regression lines defining this plot and its optimum. Uncertainties were estimated as described in section 2 above. We adopt therefore for NH_3 decomposition $E_{MN,opt} = 88.0 \pm 4$ kJ.Mol^{-1}. We notice that it is identical to $E_{MN,opt}$ for NH_3 synthesis within error margins.

Table ST.5.3: Comparison of experimental activities and calculated E_{MN} values for alumina supported transition elements catalysts of NH_3 decomposition considered in Fig. S.51. (a) Activities from ref [30] of main text, being expressed as turnover frequencies in s^{-1}.

Formula	*Space group*	*Target atom M*	*Z*	E_{MN} *(kJ.Mol^{-1})*	**Activity**
Left side					(a)
Cu_2N	Pbcn	Cu	6	69.2	1.300E-02
Pd_2N	Pnnm	Pd	6	65.5	1.94E-02
PtN_2	PMNN	Pt	6	65.8	2.26E-02
IrN_2	Pnnm	Ir	6	79.6	7.86E-01
Rh_2N	P6_3/mmc	Rh	6	77.9	2.26E+00
Ni_2N	Pbcn	Ni	6	88.6	4.21E+00
Ru_2N	P6_3/mmc	Ru	6		6.85E+00
Right side					(a)
Ru_2N	P6_3/mmc	Ru	6	93.4	6.85E+00
Co_2N	PMNN	Co	6	93.33	1.33E+00
Fe_2N	Pbcn	Fe	6	114.2	3.27E-01
Cr_2N	P-31m	Cr	6	128.2	2.20E-02

Table ST.5.4: Parameters of regression lines defining the volcano plot shown on Fig. S.5.1, for NH_3 decomposition, Intercepts b and Activity max in Activity units of s^{-1}; R^2: squared correlation coefficients; $E_{MN,opt}$ in kJ.mol^{-1}; slopes m in units of Activity.kJ^{-1}.mol.

	NH_3 decomposition left side	*NH_3 decomposition right side*
m	0.1157	-0.0588
b	-9.341	6.011
R^2	0.8679	0.903
$E_{MN,opt}$	88.0	
$\Delta E_{MN,opt}$	4 (4.6%)	
Activity max	6.9	
ΔActivity max	3.2	

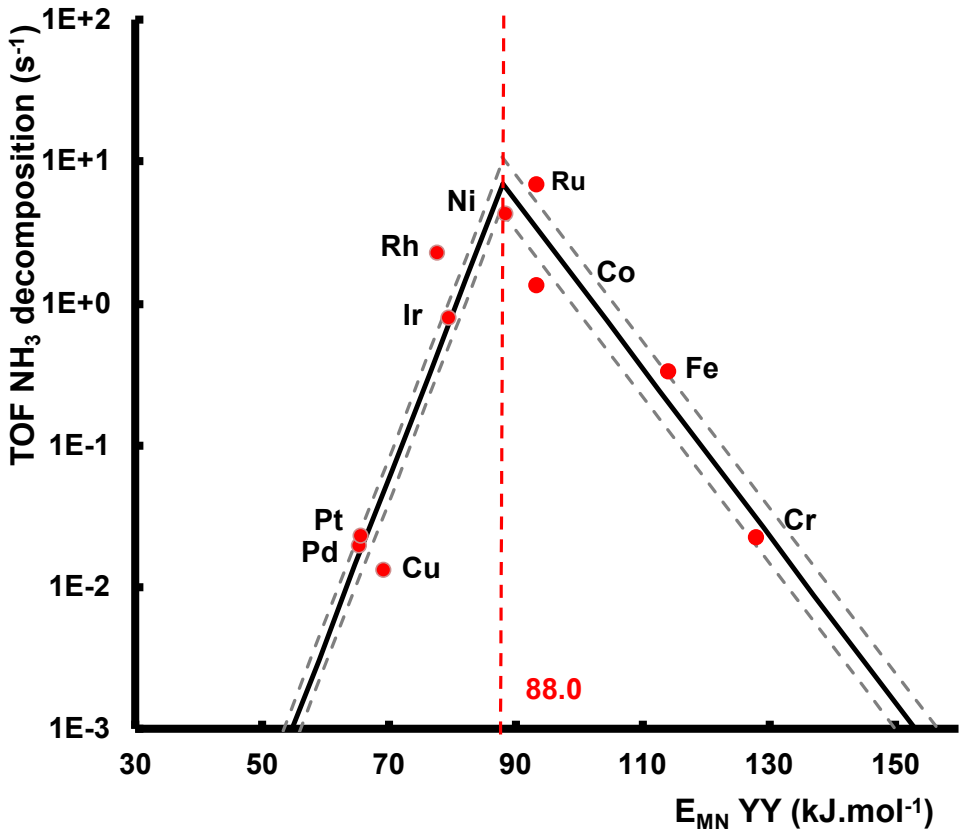

Fig. S.5.1: Volcano plot for NH_3 decomposition over alumina supported transition elements.

6- *Volcano pattern for hydrogenation of styrene into ethylbenzene, and ethene into ethane against E_{MC} in transition metal carbides*

For this case we refer to the recent reference co-authoring some of us (reference [7] of main text), which shows a (double) volcano plot for the selective hydrogenation of styrene into ethylbenzene catalyzed by silica supported transition metals The first peak of this volcano plot culminates for the abscissa $E_{MC,opt}$ = 69.5 ± 1 kJ.Mol^{-1} when E_{MC} is computed in the Fm-3m (NaCl) structure. It is as expected very close to the value $E_{MC,opt}$ = 69.0 kJ.Mol^{-1} reported for hydrogenation of ethene into ethene in ref. [3] of main text.

7- *Volcano pattern for hydrogenation of benzene against E_{MC} in transition metal carbides.*

For this case, we refer to ref. [3] of main text, which revealed a volcano plot for the hydrogenation of benzene at 303 K catalyzed by γ-alumina supported transition elements and some of their alloys. We have re-interpreted the original data using the more appropriate M_2C structures for the testing conditions, retaining the most stable structures according to computed heats of formation. $E_{MC,opt}$ are determined at the intersection of the left hand side and right hand side regression lines in a semi-log plot of activities versus E_{MC}. Table ST.7.1 presents the relevant data, and Figure S.7.1 the resulting volcano plot. Table ST.7.2 provides the parameters for the regression lines defining this plot and its optimum. We obtain $E_{MC,opt}$= 110.9 ± 1 kJ.Mol^{-1} for hydrogenation of benzene. In the case of alloys $M1_3M2$, we use the simple lever rule $E_{MC} = \left(\frac{3E_{M1C} + E_{M2C}}{4}\right)$ for the plot, but they are not included in the determination of regression lines. This procedure turns out to be fairly predictive for the activities of these alloyed catalysts.

Table ST.7.1: Comparison of experimental activities and calculated E_{MC} values for γ-alumina supported transition elements catalysts of benzene hydrogenation considered in Fig. S.7.1 (a) Activities from [3] of main text, being expressed as turnover frequencies in s^{-1}.

Formula	*Space group*	*Target atom M*	*Z*	E_{MC} *(kJ.Mol^{-1})*	**Activity**
Left side					(a)
Cu_2C	Pnnm	Cu	6	88.1	2.3
Pd_2C	P6_3/mmc	Pd	6	96.0	6.5
Pt_2C	P6_3/mmc	Pt	6	97.8	139.6
Ir_2C	P6_3/mmc	Ir	6	95.1	117.5
Os_2C	P6_3/mmc	Os	6	106.3	331.1
Cu_3IrC_4	Lever rule		6	89.9	9.1
Ir_3CuC_4	Lever rule		6	93.4	50.1
Ir_3ReC_4	Lever rule		6	102.3	389.0
Right side					(a)
Co_2C	Pnnm	Co	6	118.6	231.8
Ni_2C	Pnnm	Ni	6	122.0	56.0
Ru_2C	Pbcn	Ru	6	125.1	42.0
Re_2C	P6_3/mmc	Re	6	123.6	35.5
Re_3IrC_4	Lever rule		6	116.5	153.1

Table ST.7.2: Parameters of regression lines defining the volcano plot shown on Fig. S.7.1, for benzene hydrogenation. Intercepts b in $\log_{10}$(Activity units of s^{-1}) and Activity max in Activity units of s^{-1}; R^2: squared correlation coefficients; $E_{MC,opt}$ in $kJ.mol^{-1}$; slopes m in units of Activity.kJ^{-1}.mol.

	benzene hydrogenation left side	*benzene hydrogenation right side*
m	0.1168	-0.1241
b	-9.706	17.0
R^2	0.6603	0.8642
$E_{MC,opt}$	110.9	
$\Delta E_{MC,opt}$	1 (1%)	
Activity max	1756	
ΔActivity max	1250	

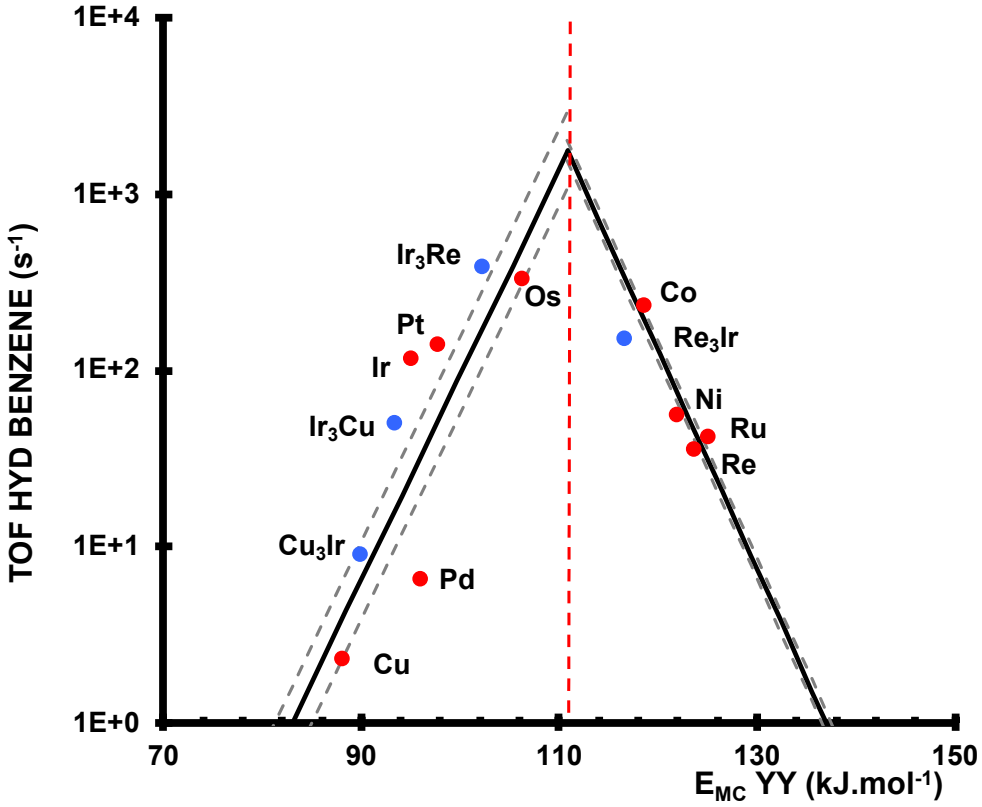

Fig. S.7.1: Volcano plot for benzene hydrogenation over γ-alumina supported transition elements (red dots) and their alloys (blue dots)

8- Volcano pattern for the methanation of carbon monoxide against E_{MC} in transition metal carbides.

Two sets of experimental data comparing the activities of supported transition metals supported are the current references for periodic trends: Bligaard et al. (ref [31] of main text) and Vannice et al. (ref. [32] of main text). For the former, transition metals are supported on an alumina stabilized magnesia (Mg/Al = 7), while they are supported on silica for the latter. While experimental conditions differ somewhat, the two sets of activities A1 (ref [31] of main text) and A2 (ref. [32] of main text) appear rather fairly correlated when expressed in mmol.molM^{-1}.s^{-1} at 550 K, and mol CH_4 produced per second per mole CO adsorbed by the used catalyst (s^{-1}) at 548 K respectively (regression equation in log-log scales : $A1 = 25.23 * (A2)^{0.606}$ with $R^2 = 0.882$).

We have estimated the stable structures of metal carbides in these testing conditions from predominance diagrams when data were available [34] or from the minimal computed heats of formation in order to discriminate between identical stoichiometries.

Table ST.8.1 presents the relevant results and Figure S.8.1 the resulting volcano plot for methanation of CO according to activity A2 (or T.O.F.). Table ST.8.2 provides the parameters for the regression lines defining this plot and its optimum. Table ST.8.3 presents the relevant results and Figure S.8.2 the resulting volcano plot for methanation of CO according to activity A1. Table ST.8.4 provides the parameters for the regression lines defining this second plot and its optimum. Both volcano plots are comparable, but activities A2, are less scattered around the left and right side regression lines. We adopt therefore for the methanation of CO the corresponding optimum: $E_{MC,opt} = 115.3 \pm 1$ kJ.Mol^{-1}.

Table ST.8.1: Comparison of experimental activities in methanation of carbon monoxide and calculated E_{MC} values for silica supported transition elements catalysts. (a) Activities A2 from ref [32] of main text being expressed as turnover frequencies in s^{-1}. (b): estimated from the correlation A2 versus A1, and not included in the volcano's right side regression line.

Formula	*Space group*	*Target atom*	*Z*	E_{MC} *(kJ.Mol^{-1})*	**Activity**
Left side					(a)
Cu_2C	Pnnm	C	6	88.1	1.5E-05
Ir_2C	P6_3/mmc	C	6	95.1	7.9E-04
Pd_2C	P6_3/mmc	C	6	96.0	3.0E-04
Pt_2C	P6_3/mmc	C	6	97.8	1.6E-03
Right side					(a)
Co_2C	Pnnm	C	6	118.7	8.7E-01
Ni_3C	R-3c	C	6	125.5	1.8E-02
Fe_2C	Pnmm	C	6	103.8	1.6E-01
Re_2C	P6_3/mmc	C	6	123.6	8.4E-03(b)
Ru_2C	Pbcn	C	6	125.1	2.7E-01
Rh_2C	Pnnm	C	6	128.5	7.3E-03

Table ST.8.2: Parameters of regression lines defining the volcano plot shown on Fig. S.8.1, for methanation of carbon monoxide, Activities A2. Intercepts b in $\log_{10}$(Activity units of s^{-1}) and Activity max in Activity units of s^{-1}. R^2: squared correlation coefficients; $E_{MC,opt}$ in $kJ.mol^{-1}$; slopes m in units of $\log_{10}$(turnover frequencies in s^{-1}).kJ^{-1}.mol.

	Methanation of CO left side	***Methanation of CO right side***
m	0.203	-0.203
b	-22.66	24.075
R^2	0.9250	0.7613
$E_{MC,opt}$	115.3	
$\Delta E_{MC,opt}$	0.8 (0.7%)	
Activity max	5.11	
ΔActivity max	1.5	

Table ST.8.3: Comparison of experimental activities in methanation of carbon monoxide and calculated E_{MC} values for alumina-MgO supported transition elements catalysts. (a) Activities A1 from ref. [31] of main text being expressed in $mmol.molM^{-1}.s^{-1}$. (b): estimated from the correlation A1 versus A2.

Formula	***Space group***	***Target atom***	Z	E_{MC} ***(kJ.Mol^{-1})***	**Activity**
Left side					(a)
Cu_2C	Pnnm	C	6	88.1	3.00E-02 (b)
Ir_2C	P6_3/mmc	C	6	95.1	6.94E-01
Pd_2C	P6_3/mmc	C	6	96.0	1.36E-01
Pt_2C	P6_3/mmc	C	6	97.8	1.26E-01
Right side					(a)
Co_2C	Pnnm	C	6	118.7	1.82E+01
Ni_3C	R-3c	C	6	125.5	3.43E+00
Fe_2C	Pnmm	C	6	103.8	3.81E+00
Re_2C	P6_3/mmc	C	6	123.6	1.30E+00
Ru_2C	Pbcn	C	6	125.1	1.82E+01
Rh_2C	Pnnm	C	6	128.5	4.09E+00

Table ST.8.4: Parameters of regression lines defining the volcano plot shown on Fig. S.8.2, for methanation of carbon monoxide, Activities A1. Intercepts b in $\log_{10}$(Activity units of s^{-1}) and Activity max in Activity units of s^{-1}. R^2: squared correlation coefficients; $E_{MC,opt}$ in $kJ.mol^{-1}$; slopes m in units of $\log_{10}$(mmol.molM-1.s^{-1}).kJ^{-1}.mol.

	Methanation of CO left side	***Methanation of CO right side***
m	0.084	-0.047
b	-8.802	6.565
R^2	0.4103	0.1193
$E_{MC,opt}$	117.0	
$\Delta E_{MC,opt}$	2.3 (2%)	
Activity max	11.4	
ΔActivity max	6.2	

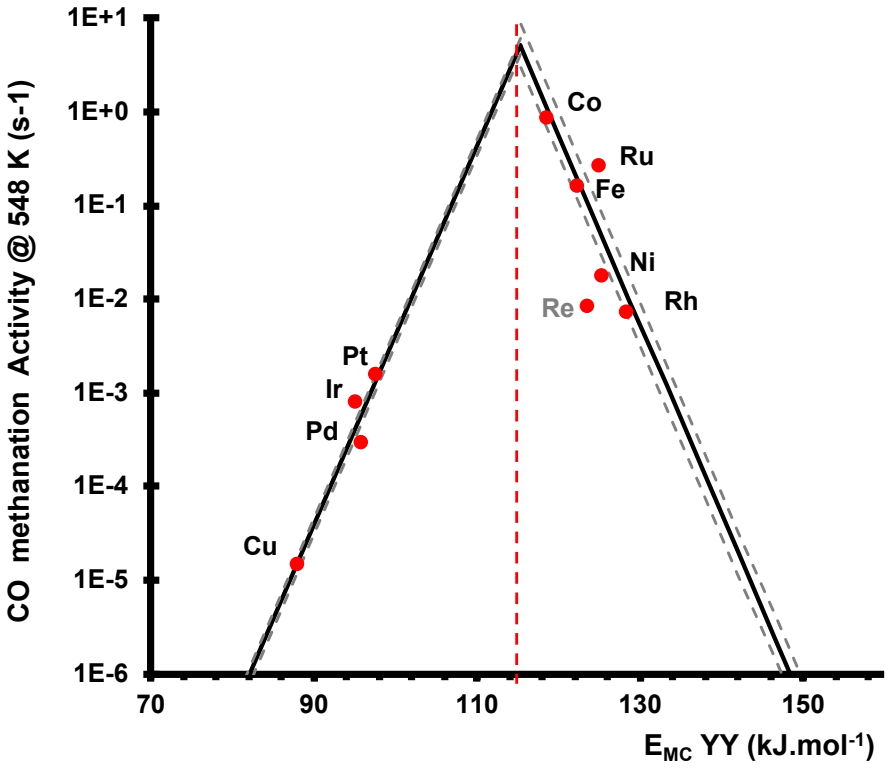

Fig. S.8.1: Volcano plot for methanation of carbon monoxide on silica supported transition elements (activities A2 from ref. [32] of main text). The activity for Re_2C is evaluated from the A2 versus A1 correlation, and not included in the determination of the right hand side regression line defining the volcano. Dotted lines bracket the regression lines by ± the standard deviation of experimental ordinates with respect to their projection on the left or right regression line, allowing estimations of error bars on the coordinates of the volcano summit as situated between cross-points of left+/right- and left-/right+.

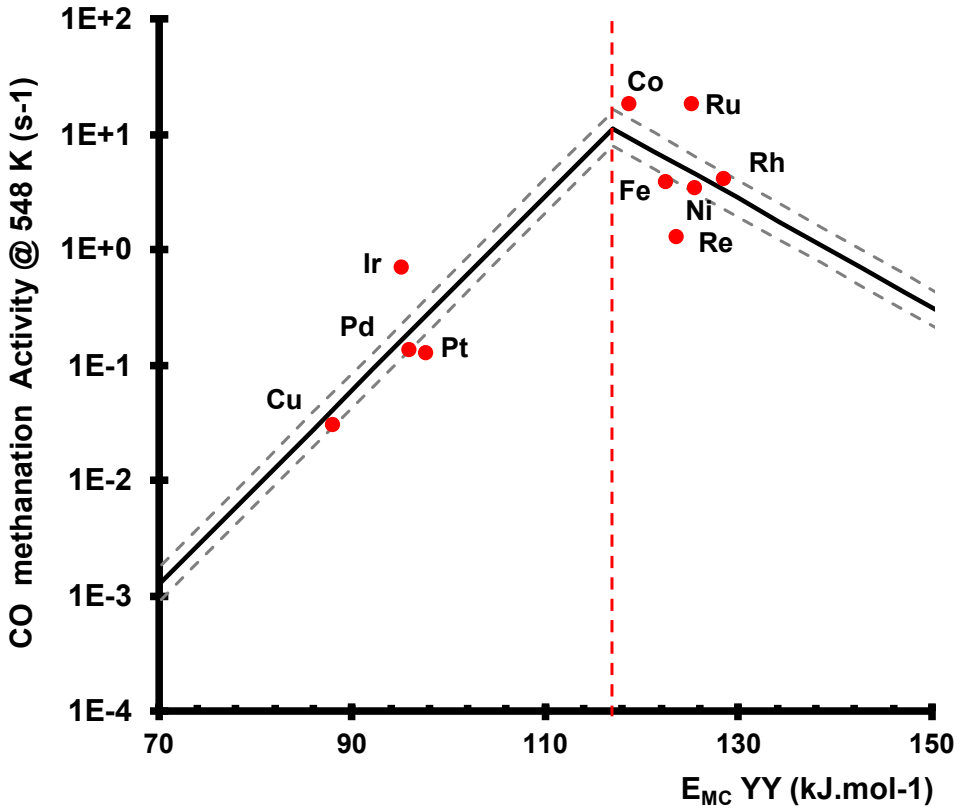

Fig. S.8.2: Volcano plot for methanation of carbon monoxide on alumina-MgO supported transition elements (activities A1 from ref. [31] of main text) The activity for Cu_2C is evaluated from the A1 versus A2 correlation. Dotted lines bracket the regression lines by ± the standard deviation of experimental ordinates with respect to their projection on the left or right regression line, allowing estimations of error bars on the coordinates of the volcano summit as situated between cross-points of left+/right- and left-/right+.

9- BEP relationship for the activation pathway of MoS_2 M-edge_50%S

In this section we provide some support to our strong hypothesis that a BEP relationship prevails for all elementary steps along a reaction pathway in adsorbed phase in realistic operating conditions. The data is available on Figure 2 of one of our recent paper (ref. [36] of main text): this figure presents the reaction pathway computed by DFT for one S vacancy creation on the M-edge 50%S of MoS_2, by heterolytic dissociative adsorption of H_2 and associative desorption of H_2S. Following the free energy change at 575 K, 10 bar H_2 and 0.1 bar H_2S, from the reference state S1 (H_2 in gas phase and the initial edge model) to S6 (H_2S in gas phase and on S vacancy on the edge) the sequence of free energy levels is listed in Table ST.10.1, and the corresponding BEP relationship presented on Figure S.9.1.

Two regression lines appear on Figure S.9.1, depending on the sign of ΔG_k when the pathway is followed from S1 towards S6. Both share approximatively the same ordinate at the origin $\Delta G_k = 0$, which may be identified as the minimal activation energy $\Delta G^{\pm}_{0}$. The absolute values of the slope differ by approximately 1, as expected, since $\Delta G_k < 0$ corresponds by convention to a direct reaction at step Sk and $\Delta G_k > 0$ to the reverse one.

Table ST.9.1: Sequence of states obtained in ref. [36] of main text for the reaction pathway computed by DFT for one S vacancy creation on the M-edge 50%S of MoS_2, by heterolytic dissociative adsorption of H_2 and associative desorption of H_2S. Free energies are in eV. The meaning of the label (Si and TSi) is given in ref. [36] of main text.

State	ΔG(575K)
S1	0
TS1	1.4
S2	0.6
TS2	1.25
S3	0.77
TS3	1.09
S4	0.45
TS4	0.89
S5	0.81
TS5	1.64
S6	0.14
TS3 bis	1.09
S3 bis	0
TS3 Ter	0.32
S4 bis	-0.24

Transition	$\Delta G^{\pm}_{k}$	ΔG_k
S1>TS1	1.4	0.6
S2>TS2	0.65	0.17
S3>TS3	0.32	-0.32
S3>TS4	0.12	0.04
S5>TS5	0.83	-0.67
S4>TS3bis	0.64	-0.45
S3bis>TS3ter	0.32	-0.24

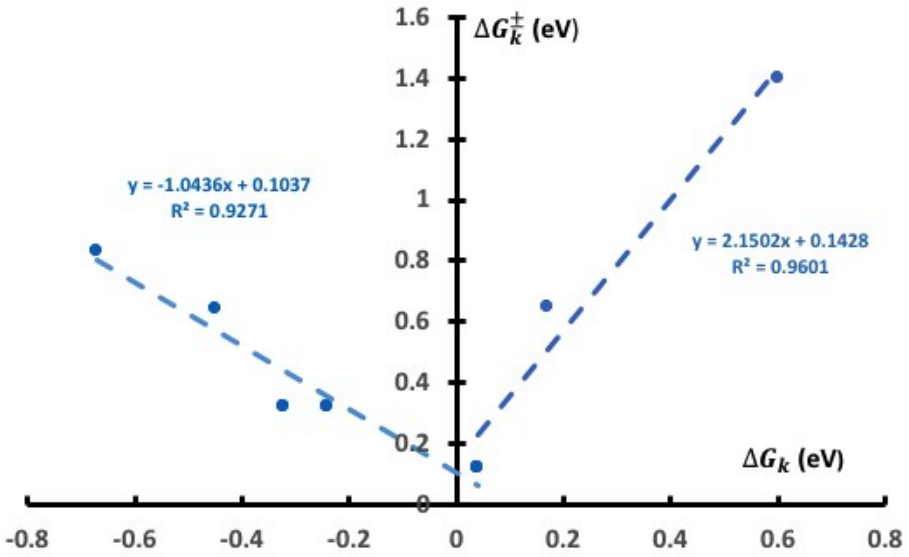

Fig. S.9.1: BEP relationship obtained for the reaction pathway computed by DFT for one S vacancy creation on the M-edge 50%S of MoS_2, by heterolytic dissociative adsorption of H_2 and associative desorption of H_2S (data from ref. [36] of main text)

10- Examples of inappropriate E_{MX} descriptors for hydrogenation reactions catalysed by transition metals

The purpose of this section is to show examples that using another descriptor than E_{MC} for hydrogenation reactions catalyzed by transition metals does not allow to construct a meaningful volcano plot. Examples given are using E_{MH} for benzene hydrogenation (Figure S.10.1 to be compared to Figure S.7.1), and using E_{MH} or E_{MO} for CO methanation (Figures S.10.2 and S.10.3 respectively to be compared to Figure S.8.1).

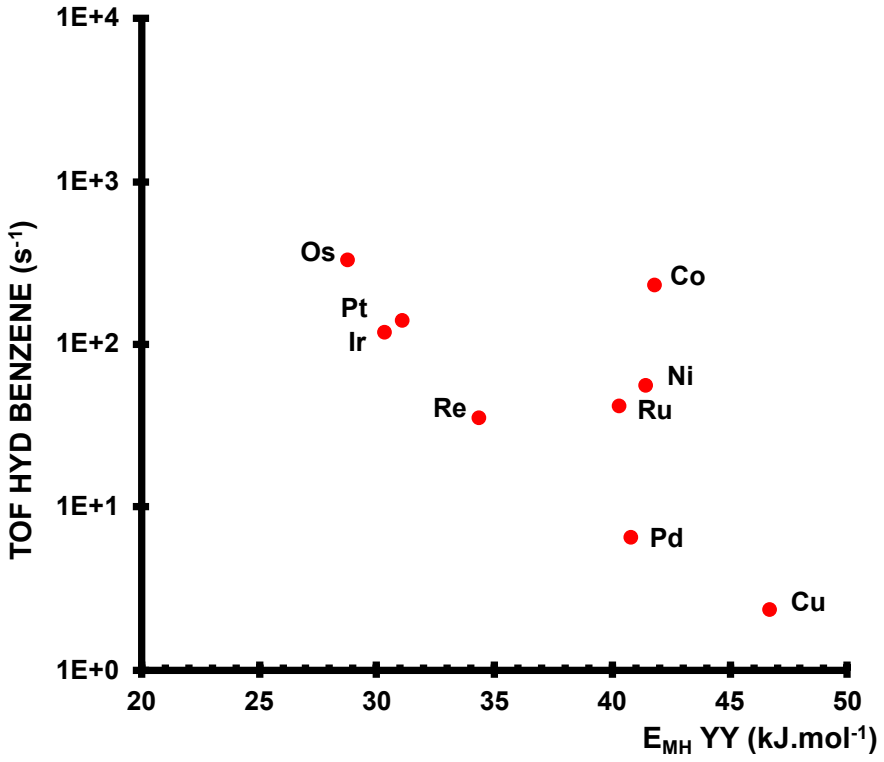

Fig. S.10.1: Plot of benzene hydrogenation activities catalyzed by γ-alumina supported transition elements (red dots) versus E_{MH} . To be compared with the volcano plot shown in Figure S.7.1 where data points have the same ordinates.

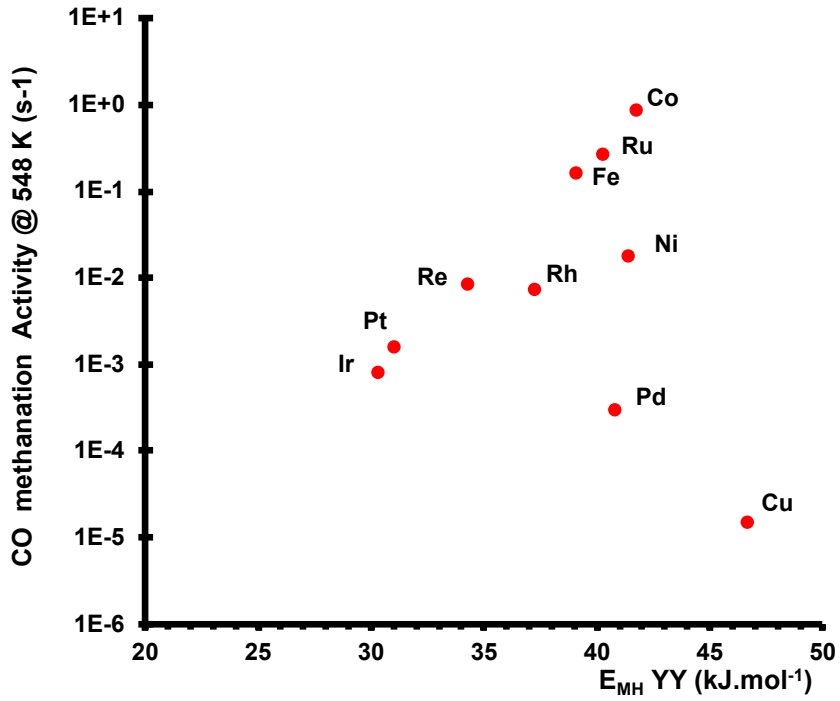

Fig. S.10.2: Plot of activities in methanation of carbon monoxide catalyzed by silica supported transition elements versus E_{MH} (activities A2 from ref. [32] of main text). To be compared with the volcano plot shown in Figure S.8.1 where data points have the same ordinates.

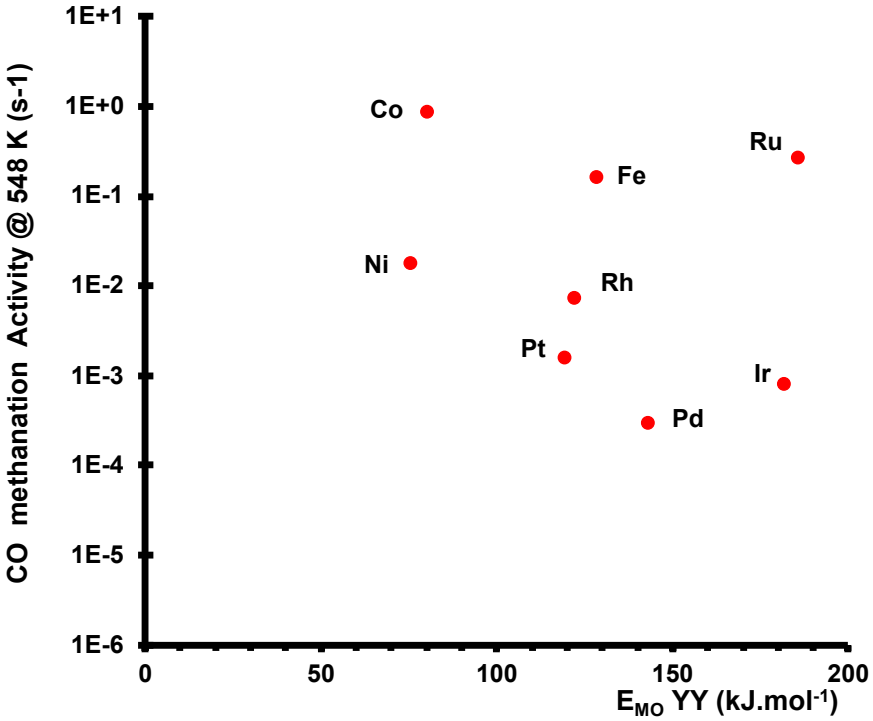

Fig. S.10.3: Plot of activities in methanation of carbon monoxide catalyzed by silica supported transition elements versus E_{MO} (activities A2 from ref. [32] of main text). To be compared with the volcano plot shown in Figure S.8.1 where data points have the same ordinates.

11 – Notice on the consistency and relevance to experimental data of Yin-Yang DFT descriptors

We are of course conscious that DFT model assumptions are liable to influence the numerical results of the Yin-Yang algorithm. In our experience however that periodic trends are correctly obtained as long as consistent levels of approximation are kept in each series of TM compounds. The magnetic state found for the Yin-Yang structures depends on the level of theory (PBE exchange functional, here which represents a reasonable compromise). Although we know that the various possible magnetic states may depend on the choice of exchange functional, our goal is not to precisely solve the magnetic ordering but rather to obtain a reasonable evaluation of the energetic values. We have observed that the latter are generally only practically independent on the cell size when a NxNxN replicate supercell is used for the Yin-Yang calculation instead of the 1x1x1 unit-cell, i.e. conserving vacancies concentrations in the Yin and Yang cell. For instance, this was the case for the model we used to represent BSCF including 100 un-equivalent Co atoms, as mentioned in section 3.1 page 9 of our manuscript: E_{CoO} computed for this model is the same as computed on $BaCoO_3$ and $ScCoO_3$ perovskites unit-cells. Finally, the founding Reference 3 of our manuscript shows rather convincing examples of linear correlations obtained between Yin-Yang descriptors and experimental heats of adsorption as for instance : i) isosteric heats of adsorption of O_2 on metals, and the theoretical descriptor E_{MO} computed in the rutile structure (R^2=0.93), ii) heats of adsorption of ethene on TMs and E_{MC} computed in the NaCl structure (R^2=0.92)